International Journal of Multidisciplinary Research and Growth Evaluation.

Enhanced Photoluminescence Performance of La ($P_{0.5}V_{0.5}$) O_4: 2 at. % Tm^{3+} Blue-Emitting Phosphors Tailored through Strategic Al^{3+} Ion Doping

Shakir Ullah [1], Xiaoli Yang [2], Xingyun Li [3*], Haoxi Be [4*], Shaukat Aziz [5]

[1, 2, 4] College of Textiles and Clothing, State Key Laboratory of Bio-Fibers and Eco-Textiles. Qingdao University, Qingdao, Shandong, China

[3] Institute of Materials for Energy and Environment, School of Materials Science and Engineering, Qingdao University, Qingdao, China

[5] Power Engineering and Engineering Thermo Physics School of Energy and Environment, Southeast University Nanjing Jiangsu China

* Corresponding Author: **Xingyun Li, Haoxi Be**

Article Info

ISSN (online): 2582-7138
Volume: 06
Issue: 02
March-April 2025
Received: 10-02-2025
Accepted: 05-03-2025
Page No: 774-783

Abstract

This study presents a comprehensive investigation into the synthesis, structural modulation, and luminescence enhancement of Al^{3+} co-doped La ($P_{0.5}V_{0.5}$) O_4:2 at. %Tm^{3+} phosphors, fabricated via a high-temperature solid-state reaction method and subjected to calcination at 1000 °C for 5 hours. These phosphors exhibit prominent blue light emission, with an intense and uniform luminescence peak centered at approximately 459 nm when excited at 359 nm. The observed emission originates predominantly from the characteristic $^1D_4 \rightarrow {}^3H_6$ electronic transition of Tm^{3+} ions, implying their preferential occupancy in highly symmetric sites within the host lattice, optimizing their radiative transition efficiency. To systematically enhance the luminescent performance of La ($P_{0.5}V_{0.5}$) O_4:2 at. %Tm^{3+}, we explored the Al^{3+} doping impact on the crystallographic structure and optical properties. The experimental results reveal that Al^{3+} incorporation induces a substantial increase in emission intensity, which follows a concentration-dependent trend initially strengthening with increasing Al^{3+} content before reaching an optimum level and subsequently declining. The maximum luminescence enhancement was achieved at an Al^{3+} doping ratio of x = 0.02 in $La_{0.96}(P_{0.5}V_{0.5})Al_{0.02}O_4$:2 at.%$Tm^{3+}$, where the emission intensity was elevated by a factor of 2.05 compared to the undoped La($P_{0.5}V_{0.5}$)O_4:2 at.%Tm^{3+} counterpart. Furthermore, these phosphors exhibit highly favorable Commission Internationale de l'Éclairage (CIE) chromaticity coordinates, well-balanced colorimetric parameters, and superior color purity, making them competitive with other reported blue-emitting rare-earth (RE)-doped phosphors. The findings highlight the potential of these phosphors for advanced applications in white light-emitting diodes (WLEDs) and next-generation optoelectronic devices, particularly in enhancing the rendering of blue-hued images in display technologies.

DOI: https://doi.org/10.54660/.IJMRGE.2025.6.2.774-783

Keywords: Al^{3+} co-doped La ($P_{0.5}V_{0.5}$) O_4:2 at. %Tm^{3+}, Solid-state method, Intense Blue-emissions, Enhanced PL properties by Al^{3+} doping

1. Introduction

As a burgeoning class within the domain of white light-emitting diodes (WLEDs), solid-state lighting (SSL) technology encompasses a multitude of compelling advantages, including exceptional luminous efficacy, prolonged operational longevity, outstanding chromatic rendering attributes, ecological sustainability, and diminished energy expenditure [1, 2, 3, 4]. Owing to these intrinsic merits, SSL is esteemed as an exceedingly promising frontier for next-generation illumination solutions and has stimulated extensive scholarly investigation alongside rapid technological advancements [5, 6, 7]. At present, three principal methodologies are employed for the fabrication of WLEDs.

The foremost approach exploits a YAG: Ce phosphor stimulated by a blue LED chip, generating yellow luminescence, which subsequently amalgamates with the residual blue emission at an optimized intensity proportion to yield white light. Nevertheless, this technique is hindered by an inherent paucity of red spectral constituents, culminating in an elevated correlated color temperature (CCT) and a diminished color rendering index (CRI), thereby adversely affecting the comprehensive quality of illumination [8, 9]. The second approach involves the integration of discrete red, green, and blue (RGB) LED chips, with their respective luminous intensities finely tuned to achieve white light emission. Despite its feasibility, this method presents significant drawbacks, including high fabrication costs due to the necessity of multiple chips and inconsistent chromatic stability caused by the varying quantum efficiencies of the different LEDs [10]. The third strategy employs ultraviolet (UV) LED excitation to stimulate blue, red, and green phosphors, enabling white light generation through precise control of the emission intensities of the three phosphors [11]. Compared to the first two methodologies, this approach offers an enhanced CRI for full-spectrum lighting and is more cost-effective. However, luminescent materials exposed to UV excitation are prone to photodegradation, compromising their longevity and stability. Consequently, to overcome these limitations, there is an urgent need to develop novel phosphor materials that exhibit efficient red, green, and blue emissions under near-UV LED excitation, ensuring both high-performance WLEDs and long-term operational stability.

Rare-earth (RE) ion-doped phosphates have garnered significant attention as promising phosphor materials due to their outstanding thermal and chemical stability, cost-effectiveness, and low phonon energy [12, 13, 14]. Their unique 4f electronic configuration enables diverse and intense emission characteristics, making them widely applicable in luminescent materials with tunable color properties. Among commercially available blue phosphors, $BaMgAl_{10}O_{17}$ doped with Eu^{2+} remains the predominant choice [15, 16]. However, alumina-based phosphors suffer from structural instability, leading to suboptimal luminous efficiency. Additionally, conventional high-temperature synthesis processes often oxide Eu^{2+} to Eu^{3+}, further compromising luminescence performance. Consequently, developing blue-light-emitting phosphors that exhibit high stability, efficient UV LED excitation, and enhanced luminous properties remains an important research direction. Among RE-based phosphors, Tm^{3+} is widely recognized as a viable blue-light-emitting activator due to its characteristic $^1G_4 \rightarrow {}^3H_6$ transition, albeit with relatively weak emission intensity. As a result, Tm^{3+} has been incorporated into various host matrices, including vanadates, fluorides, tungstates, and silicates, to optimize its emission efficiency [17, 18, 19, 20].

In parallel, RE vanadates have emerged as highly promising phosphor hosts owing to their superior luminescence efficiency, high quantum yield, and the capacity to accommodate high RE ion doping concentrations [2, 21, 22]. The VO_4^{3-} tetrahedral groups provide an ideal crystal field environment for dopant ions, exhibiting strong UV absorption and efficiently transferring the absorbed energy to RE activators [2, 23]. In a prior study, we systematically investigated the impact of VO_4^{3-} and PO_4^{3-} group substitution on the structural, luminescent, and chromatic purity properties of vanadate-based phosphors, leading to an optimized host matrix [24]. Building upon these findings, this study explores the role of Al^{3+} substitution in modulating the photoluminescence (PL) characteristics of La $(P_{0.5}V_{0.5})$ O_4:2 at. % Tm^{3+} phosphors. Integrating metal ions into the host lattice significantly improves PL properties. Here, Al^{3+} is introduced in trace amounts as a sensitizer to improve energy absorption and transfer to Tm^{3+} activators, thereby optimizing luminescence efficiency [1, 2, 25]. The impact of Al^{3+} concentration on the PL behavior and microstructural attributes of $La_{0.98-x}$ $(P_{0.5}V_{0.5})$ Al_xO_4:2 at. % Tm^{3+} $(0.0 \leq x \leq 0.04)$ phosphors were systematically evaluated. The resulting phosphor material is promising as a blue-emitting candidate for use in white light-emitting diodes (WLEDs), photovoltaic devices, and other next-generation optoelectronic technologies [24, 25].

2. Experimental procedure

2.1 Synthesis

A series of blue-emitting phosphors, activated by Tm^{3+}, was successfully synthesized through the high-temperature solid-state reaction method, labeled as $La_{0.98-x}$ $(P_{0.5}V_{0.5})$ AlxO4:2 at. %Tm^{3+}, with *x* ranging from 0.0 to 0.04. The synthesis utilized high-purity lanthanum oxide (La_2O_3), aluminum oxide (Al_2O_3), and diammonium hydrogen phosphate ($(NH_4)_2HPO_4$) with a chemical purity of 99.99% as the fundamental precursor materials. Thulium oxide (Tm_2O_3), with an identical chemical purity of 99.99%, was introduced as a dopant at a fixed concentration of 2 mol%. Comprehensive details regarding the compositional parameters and precursor materials are systematically outlined in Table 1. Initially, accurately determined stoichiometric proportions of La_2O_3, Al_2O_3, and Tm_2O_3 powders were entirely solubilized within a diluted nitric acid (HNO_3) solution to attain a uniformly dispersed and optically transparent mixture. The resultant solution was then transferred into an ample volume of distilled water and subjected to preheating at 85 °C to promote the formation of precursor species. In the ensuing stage, $(NH_4)_2HPO_4$ was incrementally introduced into the solution through a meticulously regulated dropwise addition technique, ensuring stringent control over the pH within a precisely maintained range of 7–9, as monitored via a precisely calibrated pH meter. Simultaneously, the solution was subjected to continuous and vigorous stirring at 450 rpm for one hour, ensuring homogeneity and thorough mixing. The resulting precursor precipitates were extensively rinsed using distilled water to eliminate any remaining residue impurities before being separated through centrifugation. The final phosphor materials were obtained by transferring the well-homogenized precursor mixture into a platinum crucible, followed by calcination at an elevated temperature of 1000 °C for 5 hours in a muffle furnace, completing the synthesis process.

Table 1: Precursor ratios for synthesizing Tm^{3+}activated phosphors and label for each sample.

Sample composition	Label	La_2O_3 (g)	Al_2O_3 (g)	Tm_2O_3 (g)
$La_{0.98}(P_{0.5}V_{0.5})$ O_4: Tm^{3+}	P0	3.1982	0.00	0.0786
$La_{0.97}(P_{0.5}V_{0.5})$ $Al_{0.01}O_4$: Tm^{3+}	P1	3.1882	0.01	0.0786
$La_{0.96}(P_{0.5}V_{0.5})$ $Al_{0.02}O_4$: Tm^{3+}	P2	3.1782	0.02	0.0786
$La_{0.95}(P_{0.5}V_{0.5})$ $Al_{0.03}O_4$: Tm^{3+}	P3	3.1682	0.03	0.0786
$La_{0.94}(P_{0.5}P_{0.5})$ $Al_{0.04}O_4$: Tm^{3+}	P4	3.1582	0.04	0.0786
NHO_3 = 25 ml, $(NH_4)_2HPO_4$ = 90ml				

2.2 Techniques of Characterization

The phase purity and crystallographic attributes of the synthesized phosphors were meticulously assessed through X-ray diffraction (XRD) analysis utilizing a Bruker D8 Advance diffractometer integrated with Cu Kα radiation (λ = 0.15406 nm). The diffraction profiles were recorded at a scanning velocity of 3°/min over a 2θ angular span ranging from 10° to 70°. The resultant phosphors' surface topology and microstructural configurations were scrutinized via scanning electron microscopy (SEM) using a high-resolution JSM-7800F microscope. Identifying functional groups within the synthesized phosphors was conducted through Fourier-transform infrared (FT-IR) spectroscopy employing a PerkinElmer FT-IR-100 spectrometer. The optical attributes, including photoluminescence (PL) emission spectra and excitation dynamics at ambient temperature, were comprehensively examined using an F-4600 fluorescence spectrophotometer. The elemental composition of the phosphors was precisely determined via inductively coupled plasma-optical emission spectroscopy (ICP-OES) using a PerkinElmer Optima 8000 spectrometer. For precise quantitative analysis, an accurately weighed 0.1 g portion of the phosphor sample was dissolved in 10 mL of concentrated hydrochloric acid (37%) and subjected to thermal digestion at 120°C for 180 minutes. Upon completion of the digestion process, the resultant solution was systematically diluted, and the concentrations of La^{3+} and Al^{3+} ions were precisely quantified.

3. Results and discussion

3.1 XRD and phase identification

The synthesized phosphors' phase integrity and crystalline nature were rigorously examined through X-ray diffraction (XRD) analysis. The diffraction profiles illustrated in Fig. 1(a) correspond to the $La_{0.98-x}$ $(P_{0.5}V_{0.5})$ $AlxO_4$:2 at. % Tm^{3+} (x = 0.0, 0.01, 0.02, 0.03, and 0.04) phosphor specimens. The XRD findings unequivocally validate the formation of a pure monoclinic phase across all synthesized compositions. As delineated in Fig. 1(a), the diffraction patterns of the phosphor samples exhibit remarkable agreement with the reference $LaVO_4$ phase (JCPDS No. 70-0216), with no discernible evidence of secondary or impurity phases. The crystallographic characteristics of the $La_{0.98-x}$ $(P_{0.5}V_{0.5})$ $AlxO_4$: Tm^{3+} powders closely parallel those of the Al^{3+} free La $(P_{0.5}V_{0.5})$ $AlxO_4$: Tm^{3+} signifying that the incorporation of Al^{3+} ions transpires through substitution at La^{3+} lattice positions. This ionic substitution engenders a stable solid solution without inducing a substantial alteration in the fundamental crystal framework. With an increasing concentration of Al^{3+}, a systematic shift in the XRD peaks toward higher diffraction angles is observed, signifying a contraction in the lattice parameters. This phenomenon arises due to the comparatively smaller ionic radius of Al^{3+} (0.535 Å) relative to La^{3+} (1.06 Å). Under Bragg's equation, $2d\sin\theta = n\lambda$, a diminution in interplanar spacing (d) is expected when nλ remains invariant, thereby leading to an elevation in the diffraction angle (θ). Consequently, the subtle displacement of the diffraction peaks substantiates the successful incorporation of Al^{3+} ions into the La^{3+} sites within the crystalline matrix [26, 27, 28, 29, 30, 31, 32, 33, 34, 35, 36].

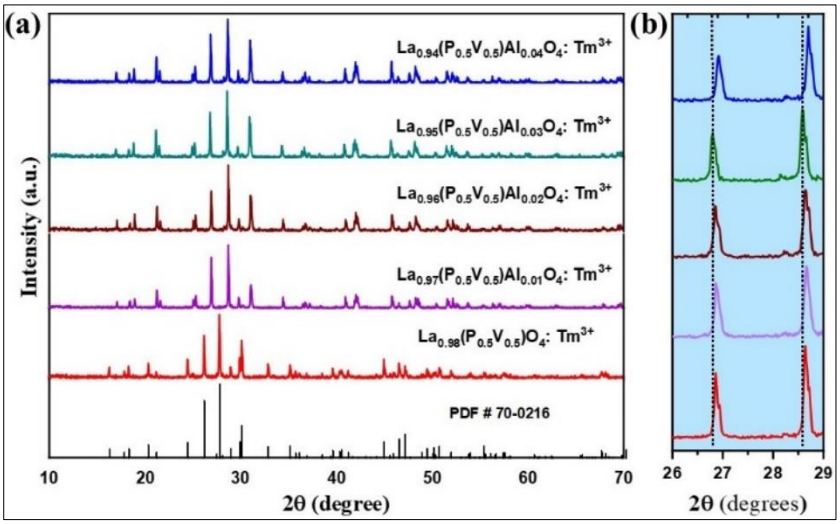

Fig 1: (a) XRD patterns of $La_{0.98-x}$ $(P_{0.5}V_{0.5})$ $AlxO_4$: Tm^{3+} (x = 0.0, 0.01, 0.02, 0.03, 0.04) and (b) enlarged patterns in the 2θ range 26°–29°.

3.2 Fourier transforms infrared spectroscopy

Fig. 2 displays the Fourier-transform infrared (FT-IR) spectrum of $La_{0.98-x}$ $(P_{0.5}V_{0.5})$ $AlxO_4$: 2 at. %Tm^{3+} phosphors. The spectral profile reveals that the predominant absorption peaks are at approximately 531 cm^{-1}, 614 cm^{-1}, and 988 cm^{-1}. Significantly, the absorption band around 988 cm^{-1}

corresponds to the asymmetric stretching vibration (v_3) of the PO_4^{3-} group. Moreover, the phosphors exhibit distinct absorption features near 743 cm^{-1} and 432 cm^{-1}, ascribed to the bending vibration of the O–V–O bond and the stretching vibration of the La–O bond, which correlates with the v_4 vibrational mode of the PO_4^{3-} group, respectively [4, 37]. In La $(P_{0.5}V_{0.5})$ O_4:2 at. $\%Tm^{3+}$ phosphors, the manifestation of two separate absorption peak sets corresponding to PO_4^{3-} and VO_4^{3-} substantiates the successful incorporation of VO_4^{3-} groups into the $LaPO_4$ crystalline matrix. The synthesized phosphors demonstrate exceptional phase purity, validated by the absence of extraneous absorption bands associated with other functional groups. Additionally, as depicted in Fig. 2, variations in Al^{3+} concentration do not induce a discernible shift in the positions of the absorption bands, further affirming the high structural purity of the synthesized samples.

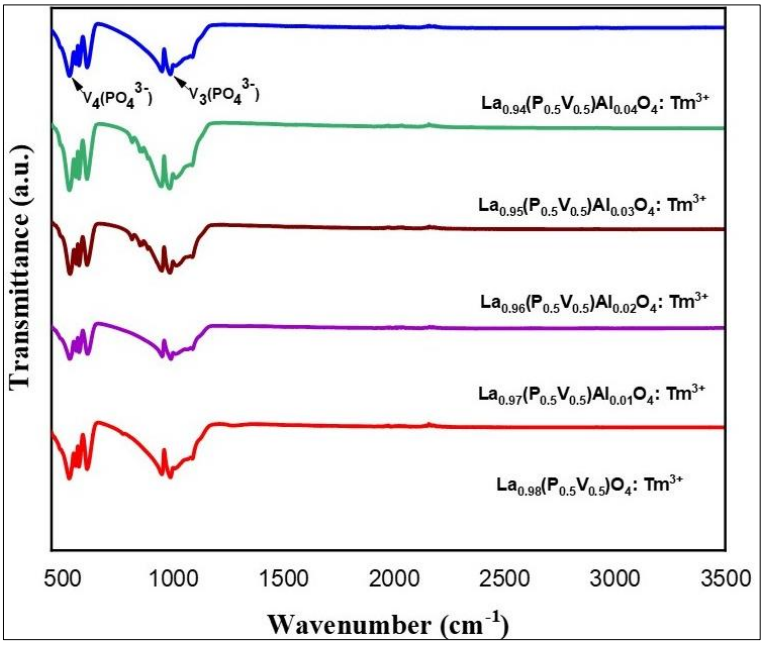

Fig 2: FT-IR spectra of $La_{0.98-x}$ $(P_{0.5}V_{0.5})$ $AlxO_4$: Tm^{3+}(x = 0.0, 0.01, 0.02, 0.03 and 0.04) phosphors series.

3.3 Field emission scanning electron microscopy

The field emission scanning electron microscopy (FE-SEM) images of the annealed $La_{0.98-x}(P_{0.5}V_{0.5})Al_xO_4$:2 at.$\%Tm^{3+}$ phosphor powders, subjected to thermal treatment at 1000 °C, are depicted in Fig. 3 for varying Al^{3+}concentrations (x = 0.0, 0.01, 0.02, 0.03, 0.04). The obtained micrographs reveal that the high-temperature annealing process induces pronounced particle agglomeration within the synthesized samples. SEM imaging was conducted on the optimized phosphor samples to systematically Explore the impact of Al^{3+} ion concentration on the morphological characteristics of the material. Fig. 2(a, b) presents the SEM images of Al^{3+} substituted La $(P_{0.5}V_{0.5})$ O_4:2 at. $\%Tm^{3+}$ phosphors at varying doping levels, elucidating their respective morphological features. A significant fraction of the phosphor particles exhibits a truncated trapezoidal crystalline grain structure. Furthermore, grain size and particle diameter irregularities are observed, indicating morphological inconsistencies. Significantly, the phosphors treated at 1000 °C display unique surface topographies, measuring about 5 µm in average length and width. As the concentration of Al^{3+} ions increase, the particle size of the annealed $La_{0.98-x}$ $(P_{0.5}V_{0.5})$ $AlxO_4$: Tm^{3+} phosphor powders show slight variations. Consequently, the size evolution of La $(P_{0.5}V_{0.5})$ O_4: Tm^{3+} phosphors follows a comparable trend to that observed for $La_{0.94}(P_{0.5}V_{0.5})$ $Al_{0.04}PO_4$: Tm^{3+}phosphor powders.

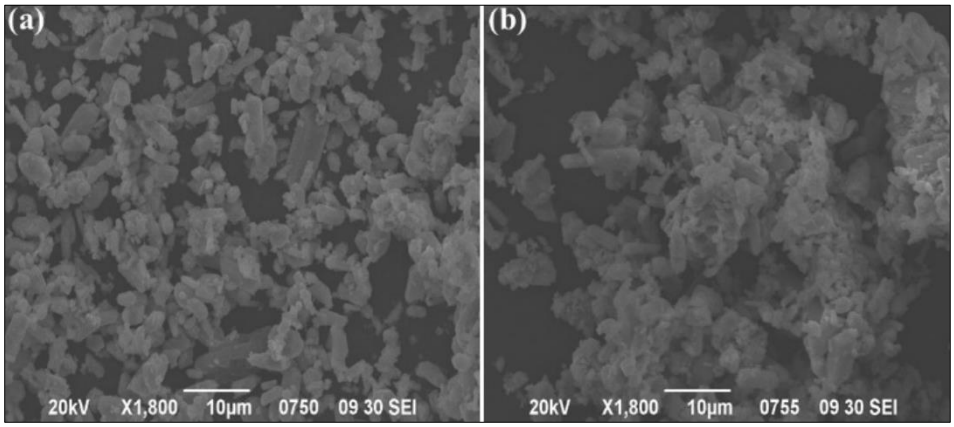

Fig 3: FE-SEM images of (a) La $(P_{0.5}V_{0.5})$ O_4: Tm^{3+} and (b) $La_{0.96}(P_{0.5}V_{0.5})$ $Al_{0.02}O_4$: Tm^{3+} phosphors.

3.4 Characteristics of photoluminescent spectroscopy

The PL excitation spectra of $La_{0.98-x}$ ($P_{0.5}V_{0.5}$) $AlxO_4$:2 at. % Tm^{3+} (x = 0.00, 0.01, 0.02, 0.03, and 0.04) phosphors, synthesized for emission in the near-ultraviolet (NUV) spectral region, manifest a broad excitation profile with a distinct peak centered at approximately 355 nm. This prominent peak arises due to the electronic transition $^3H_6 \rightarrow {}^1D_2$ within Tm^{3+} ions, as depicted in Fig. 4. Additionally, a comparatively weaker peak emerges near 360 nm, likely attributed to non-radiative energy transfer mechanisms. The transition $^3H_6 \rightarrow {}^1D_2$ denotes the direct excitation of Tm^{3+} ions from their fundamental state to an energetically elevated state [38]. Notably, the observed excitation wavelength optimizes with NUV LED chips, underscoring its potential for practical photonic applications. The pronounced $^3H_6 \rightarrow {}^1D_2$ transition at 355 nm has been systematically utilized as the excitation source for acquiring the corresponding emission spectra [39, 40]. Furthermore, the PL excitation spectra of the synthesized phosphors exhibit a broad spectral range, signifying proficient energy absorption and subsequent transfer. The luminescence mechanism is fundamentally governed by the charge transfer (CT) transition occurring within the VO_4^{3-} moiety, wherein electron transitions from the oxygen 2p (O–2p) orbitals to the vanadium 3d (V–3d) orbitals take place. This mechanism remains consistent with previously reported vanadium-based phosphors [40]. The electronic configuration of V^{5+} ions, characterized by tetrahedral (T_d) symmetry, comprises a fundamental $^1A_1$ ground state and multiple excited states, including $^1T_1$, $^1T_2$, $^3T_1$, and $^3T_2$, as illustrated in Fig. 6. Within the PL excitation spectra, absorption bands correspond to charge transfer transitions from the $^1A_1$ ground state to the excited $^1T_2$ and $^3T_2$ states within the VO_4^{3-} framework [41]. Upon excitation of the VO_4^{3-} group, the resultant charge transfer from the O^{2-} ligand to the V^{5+} center induces extensive broadband absorption, followed by energy migration to Tm^{3+} ions [42]. Initially, the host matrix absorbs energy and transfers it to the dopant ions, facilitating photoluminescent behavior. For the synthesized $LaPO_4$ phosphors, which crystallize in a monoclinic lattice system, La^{3+} ions are coordinated by nine oxygen atoms, with an average La–O bond length of 0.2611 nm. This coordination state contrasts with the hexagonal lattice arrangement, wherein La^{3+} ions exhibit eight-fold coordination, characterized by a reduced La–O bond length of 0.2497 nm [43, 44]. Consequently, a subtle blue shift in the charge transfer band is discernible. Moreover, as illustrated in Fig. 4, the PL excitation spectra display a broad excitation band arising from the charge transfer transition $O^{2-} \rightarrow Tm^{3+}$. This phenomenon occurs as electrons populate the partially filled 2p orbital of O^{2-} and the 4f orbital of Tm^{3+}, thereby modulating the luminescence characteristics of the phosphor material.

Incorporating Al^{3+} ions into the La ($P_{0.5}V_{0.5}$) O_4: 2at. % Tm^{3+} phosphor does not induce any discernible shift in the positions of the excitation peaks. Nevertheless, it markedly amplifies the intensity of the Tm^{3+} excitation peaks, signifying its potential to enhance the luminescent characteristics of the material. In the ultraviolet excitation spectra of $La_{0.98-x}$ ($P_{0.5}V_{0.5}$) $AlxO_4$: 2 at. % Tm^{3+} phosphors, particularly within the 355 nm region, this intensification is attributed to the charge transfer transition from O^{2-} to Tm^{3+}. This phenomenon transpires as valence electrons from oxygen ligands are transferred to the unoccupied orbitals of the metal cations [4, 45]. The introduction of additional metal ions significantly enhances both the absorption capability of the host lattice and the charge transfer transition from O^{2-} to Tm^{3+}. These metal ions act as mediators, facilitating the efficient excitation energy transfer from the host lattice to the Tm^{3+} activator [46]. Consequently, this mechanism leads to a pronounced increase in emission intensity. Comparable enhancements in luminescence have been observed in Tm^{3+} and metal (M)-co-doped $Ca(Y_{1-x-y}M_xEu_y)$ BO_4 (where M represents Zn, La, and Al) phosphors at specific compositions of (x = 0.0, 0.1; y = 0.04, 0.13). Notably, $Ca(Y_{0.915}M_{0.25}Eu_{0.06})$ BO_4 phosphors (with M being Zn, La, and Al) exhibited substantially higher emission intensities than their counterparts doped solely with Eu^{3+}, specifically $Ca(Y_{0.94}Eu_{0.06})$ BO_4 phosphors [47].

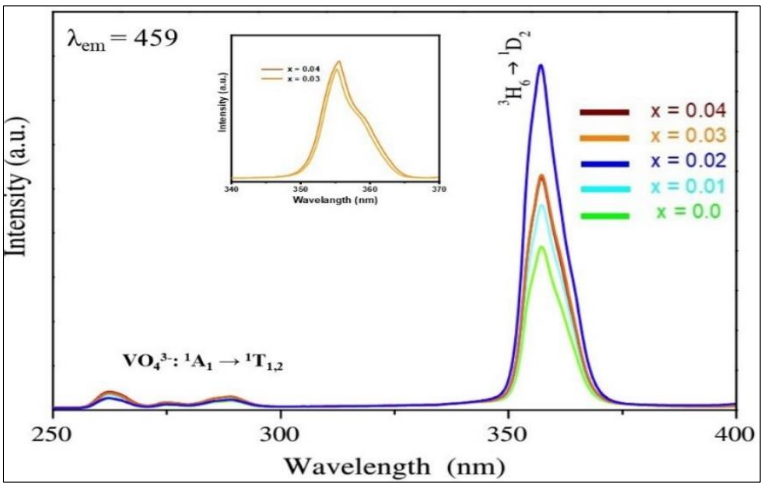

Fig 4: PL excitation spectra of $La_{0.98-x}(P_{0.5}V_{0.5})Al_xO_4$: Tm^{3+} (x = 0.0, 0.01, 0.02, 0.03, 0.04) phosphors series.

Upon excitation at 355 nm, the PL spectrum reveals a dominant emission peak at 459 nm, signifying the characteristic blue luminescence of Tm^{3+}, which originates from the electronic transition $^1D_2 \rightarrow {}^3F_4$. A relatively weaker emission peak appears around 476 nm, corresponding to the $^1D_2 \rightarrow {}^3F_4$ transition of Tm^{3+}. The emission at 476 nm arises due to residual multi-phonon-assisted non-radiative relaxation from the $^1D_2 \rightarrow {}^3F_4$ level. The observed emission

peaks fall within the blue spectral region, affirming that the synthesized phosphor powder exhibits prominent blue luminescence. Moreover, a distinct spectral band emerges near 430 nm, likely attributable to electronic transitions within the VO_4^{3-} group. This assignment is substantiated by its proximity to the characteristic transitions $^3T_2 \rightarrow {}^1A_1$ (411 nm) and $^3T_1 \rightarrow {}^1A_1$ (432 nm). The underlying energy transfer mechanisms governing these luminescent processes are depicted in Fig. 6 [48].

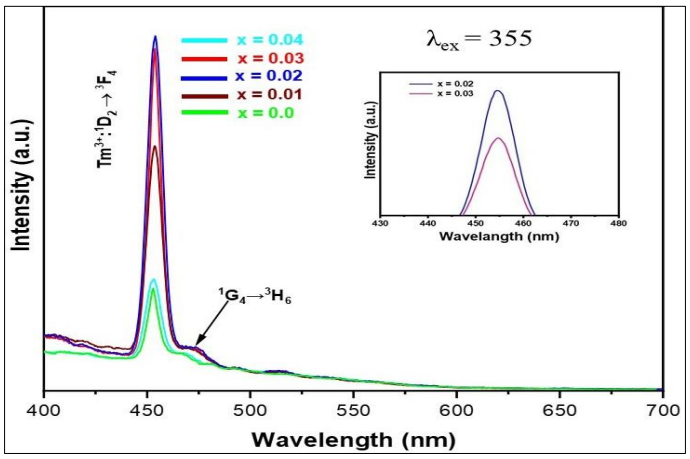

Fig 5: PL emission spectra of $La_{0.98-x}(P_{0.5}V_{0.5})Al_xO_4$: Tm^{3+} (x = 0.0, 0.01, 0.02, 0.03, 0.04) under 355 nm excitation.

For La $(P_{0.5}V_{0.5})$ O_4:2 at. % Tm^{3+} phosphors, the intensity of both PL excitation and emission experiences a substantial enhancement with increasing Al^{3+} concentration, while the spectral profile remains largely unchanged. However, the emission intensity continues to exhibit an upward trend. At an Al^{3+} concentration of x = 0.02 mol%, the phosphors show a significant rise in excitation and emission intensities. This enhancement can be attributed to efficient energy transfer between activator ions, facilitated by the presence of the VO_4^{3-} group [49]. Notably, the emission intensity of $La_{0.96}(P_{0.5}V_{0.5})$ $Al_{0.02}O_4$:2 at. % Tm^{3+} phosphors is approximately 16 and 2.2 times higher than La $(P_{0.5}V_{0.5})$ O_4:2 at. % Tm^{3+} phosphors, respectively [50, 51].

Integrating Al^{3+} into the host lattice boosts the charge transfer band intensity of $O^{2-} \rightarrow Tm^{3+}$ due to the notably smaller ionic radius of Al^{3+} (0.535 Å). This phenomenon enhances the charge transfer interactions between O^{2-} ions doped with Al^{3+} and Tm^{3+} ions. The reduced ionic radius of Al^{3+}, in contrast to La^{3+}, induces localized structural distortions upon substitution for the larger La^{3+} ions. Despite these distortions, the overall unit cell dimensions remain unaffected. The resultant structural asymmetry around Tm^{3+} ions amplifies the $^1D_2 \rightarrow {}^3F_4$ blue emission at 459 nm, a feature characteristic of asymmetric environments. However, beyond a critical Al^{3+} concentration, a decline in emission intensity is observed. This attenuation is attributed to excessive energy transfer among Tm^{3+} ions, dissipating via non-radiative transitions rather than contributing to visible light emission. The prevalence of non-radiative transitions at elevated Al^{3+} concentrations is crucial for comprehending the fundamental excitation mechanisms and optimizing material performance for technological applications [45]. The underlying causes of this non-radiative energy dissipation at high Al^{3+} levels can be ascribed to: (1) the creation of Al^{3+} clusters that serve as energy sinks because of decreased interionic spacing; (2) the reduced efficiency of energy transfer from Al^{3+} to Tm^{3+} compared to Al^{3+} to Al^{3+} energy transfer; and (3) the diminished ability of Al^{3+} ions to sensitize Tm^{3+} emission bands [52, 53]. Analogous phenomena have been documented in $GdVO_4$: Bi^{3+}, Eu^{3+} and $CaWO_4$: Bi^{3+}, Eu^{3+} systems, where Eu^{3+}emission intensity demonstrated a sharp increase with Bi^{3+} concentration up to 0.05–0.2 mol% before declining at higher Bi^{3+} levels. Furthermore, in $GdVO_4$: Bi^{3+}, Eu^{3+}, emission intensity rose significantly until reaching 0.5 mol%, after which it stabilized. The highest emission intensity occurred at a Bi^{3+} concentration of 0.5 mol%. [54, 55].

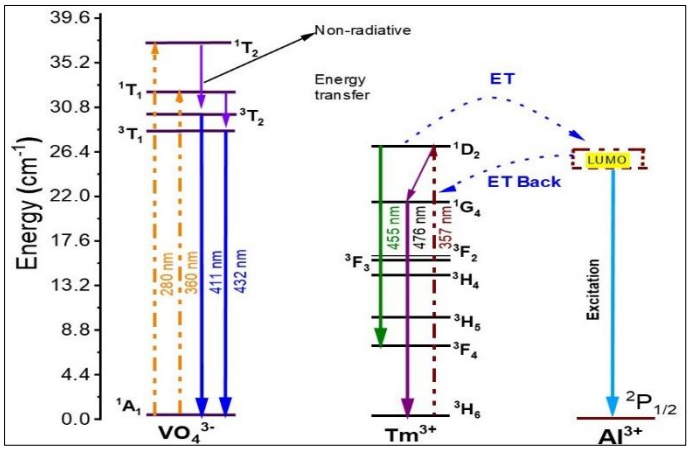

Fig 6: Energy level diagram and energy transfer processes of La $(P_{0.5}V_{0.5})$ O_4: Tm^{3+} and Al^{3+}.

3.5 CIE chromaticity coordinates and purity

The chromaticity coordinates established by the Commission Internationale de l'Éclairage (CIE) are essential for assessing the optical characteristics of synthesized phosphors. The precise CIE chromaticity coordinates for $La_{0.98-x}(P_{0.5}V_{0.5})Al_xO_4$:2 at.% Tm^{3+} (x = 0.0, 0.01, 0.02, 0.03, 0.04) were meticulously extracted from the PL emission spectra under excitation at 355 nm. The derived chromaticity data are systematically illustrated in Fig. 7 and Table 2. A detailed examination of the chromaticity diagram unequivocally establishes that the synthesized phosphors' (x_s, y_s) coordinates are firmly within the blue spectral domain. To elucidate the influence of Al^{3+} substitution on the luminescent characteristics of the phosphors, the color purity of the emitted blue light was rigorously quantified through the following mathematical formulation [56].

$$\text{Color purity} = \frac{\sqrt{(x_s - x_{ee})^2 - (y_s - y_{ee})^2}}{\sqrt{(x_d - x_{ee})^2 + (y_d - y_{ee})^2}} \times 100$$

Where (x_s, y_s) correspond to the chromaticity coordinates of the synthesized phosphors, (x_{ee}, y_{ee}) represent the equal-energy white point (0.3101, 0.3162) under Illuminant C, and (x_d, y_d) denote the dominant wavelength coordinates. By employing this equation, the computed color purity values for the synthesized phosphors are systematically compiled in Table 2. Notably, the findings reveal that the phosphors exhibit an exceptionally high color purity, peaking at 95.66% when x = 0.02.

Table 2: CIE coordinates and color purity of $La_{0.98-x}$ ($P_{0.5}V_{0.5}$) $AlxO_4$:2 at. % Tm^{3+} phosphors.

Samples	CIE Coordinates		Color purity (%)
	x_s	y_s	
P0	0.1434	0.0331	78.42
P1	0.1466	0.0566	79.51
P2	0.1583	0.0597	95.66
P3	0.1611	0.1562	92.29
P4	0.1601	0.1328	80.94

Furthermore, the meticulously calculated CIE chromaticity coordinates, color purity values, and dominant wavelengths for each phosphor composition have been comprehensively documented. The results unequivocally confirm that the Al^{3+} doped La ($P_{0.5}V_{0.5}$) O_4:2 at. % Tm^{3+} phosphor emits within the blue spectral region, with a dominant wavelength of 459 nm. The remarkably high color purity (~95.66%) powerfully underscores its potential as a viable candidate for commercial blue phosphor applications, positioning it as a compelling alternative to well-established $BaMgAl_{10}O_7:Eu^{2+}$ phosphors and previously reported $NaSrBO_3$: Ce^{3+} and $KMgBO_3$: Tm^{3+} blue phosphors [4, 7, 57, 58]. Additionally, the synthesized phosphors exhibit high spectral similarity to $NaSrPO_4$: Tm^{3+} and Gd ($P_{0.1}V_{0.9}$) O_4:1 at. %Tm^{3+} phosphors have recently garnered considerable research attention [4, 57, 59]. These compelling findings substantiate the immense potential of the developed phosphors as next-generation blue-emitting materials for light-emitting diode (LED) applications [4, 14, 58].

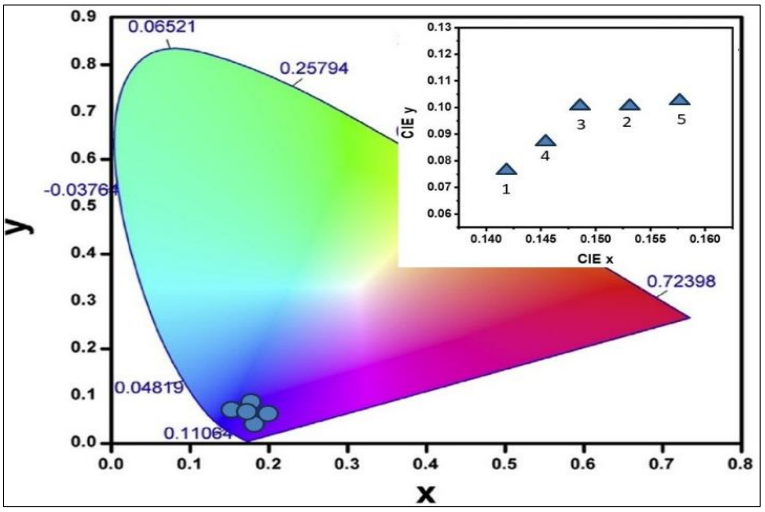

Fig 7: CIE chromaticity diagram of the $La_{0.98-x}$ ($P_{0.5}V_{0.5}$) $AlxO_4$: Tm^{3+} phosphors excitation at 355 nm.

4. Conclusion

In summary, Al^{3+} ions are incorporated into La ($P_{0.5}V_{0.5}$) O_4:2 at. % Tm^{3+} phosphors significantly enhance their luminescent properties. The optimal Al^{3+} concentration is x = 0.02 mol%, resulting in a 16-fold increase in emission intensity compared to the undoped phosphor. This enhancement is attributed to the efficient energy transfer from the VO_4^{3-} group to the Tm^{3+} ions, facilitated by the smaller ionic radius of Al^{3+}. However, excessive Al^{3+} concentration leads to decreased emission intensity due to the forming of Al^{3+} aggregates and reduced energy transfer efficiency. This study's findings offer important insights for designing and optimizing phosphors suitable for solid-state lighting and display technologies.

Declaration of competing interest

The authors declare that they have no known competing financial interests or personal relationships that could have appeared to influence the work reported in this paper.

Data availability

Data will be made available on request.

5. Acknowledgments

The authors gratefully acknowledge the Shandong provincial colleges and universities youth innovation technology support program (No. 2023KJC029), Shandong Taishan Scholars Project (No. ts20190932), State Key Laboratory of Bio-Fibers and Eco-Textiles, Qingdao University (No. G2RC202021) for support.

6. References

1. Priya R, Mariappan R, Karthikeyan A, Palani E, Krishnamoorthy E, Gowrisankar G. Review on rare earth metals doped LaPO4 for optoelectronic applications. Solid State Communications. 2021 Nov 1;339:114457. doi: 10.1016/j.ssc.2021.114457.
2. Wu X, Bai W, Hai O, Ren Q, Zheng J, Ren Y. Tunable color of *Tb3+/*Eu3+/*Tm3+-coactivated K3La(PO4)2 via energy transfer: A single-phase white-emitting phosphor. Optics & Laser Technology. 2019 Jul 1;115:176-85. doi: 10.1016/j.optlastec.2019.02.021.
3. Tymiński A, Śmiechowicz E, Martín IR, Grzyb T. Ultraviolet- and near-infrared-excitable LaPO4:Yb3+/*Tm3+/*Ln3+ (Ln = Eu, Tb) nanoparticles for luminescent fibers and optical thermometers. ACS Applied Nano Materials. 2020 Jul 24;3(7):6541-51. doi: 10.1021/acsanm.0c01025.
4. Liu Y, Huang C, Wang J, Wang Y, Wang Y. Blue emission and color-tunable behavior in Tm3+ singly- and *Dy3+/*Tm3+ co-doped CaLaGa3O7 phosphors. Ceramics International. 2024 Jun 15;50(12):21304-10. doi: 10.1016/j.ceramint.2024.03.240.
5. Peng M, Yin X, Tanner PA, Brik MG, Li P. Site occupancy preference, enhancement mechanism, and thermal resistance of Mn4+ red luminescence in Sr4Al14O25: Mn4+ for warm WLEDs. Chemistry of Materials. 2015 Apr 28;27(8):2938-45. doi: 10.1021/acs.chemmater.5b00226.
6. Xu D, Zhou W, Zhang Z, Ma X, Xia Z. Luminescence property and energy transfer behavior of apatite-type Ca4La6(SiO4)4(PO4)2O2: Tb3+, Eu3+ phosphor. Materials Research Bulletin. 2018.
7. Li Y, Zheng J, Li Z, Yang X, Chen J, Chen C. Luminescence properties of NaSrPO4: Tm3+ as novel blue-emitting phosphors with high color purity. Optik. 2018 Sep 1;169:257-63. doi: 10.1016/j.ijleo.2018.05.065.
8. Brik MG, Pan YX, Liu GK. J. Alloy. Compd. 2011;509:1452.
9. Wu H, Zhang L, Zeng X, Lei L. Improving phosphorescence of Sr2MgSi2O7: Eu2+ phosphor by Tm3+ co-doping for AC-LEDs. Optical and Quantum Electronics. 2024 Nov 10;56(11):1849. doi: 10.1007/s11082-024-06583-5.
10. Tanner PA, Pan ZF. Inorg. Chem. 2009;48:11142.
11. Xu D, Zhou W, Zhang Z, Ma X, Xia Z. Luminescence property and energy transfer behavior of apatite-type Ca4La6(SiO4)4(PO4)2O2: Tb3+, Eu3+ phosphor. Materials Research Bulletin. 2018 Dec 1;108:101-5. doi: 10.1016/j.materresbull.2018.08.040.
12. Wang X, Du F, Wei D, Huang Y, Seo HJ. The blue-emitting phosphor of Eu2+-doped Ca2Sr(PO4)2. Journal of The Electrochemical Society. 2011;158.
13. Vidican I, Smith MD, zur Loye HC. Crystal growth, structure determination, and optical properties of new potassium-rare-earth silicates K3RESi2O7 (RE = Gd, Tb, Dy, Ho, Er, Tm, Yb, Lu). Journal of Solid State Chemistry. 2003 Feb 1;170(2):203-10. doi: 10.1016/S0022-4596(02)00029-4.
14. Brow RK, Kirkpatrick RJ, Turner GL. Nature of alumina in phosphate glass: II, Structure of sodium alurninophosphate glass. J. Am. Ceram. Soc. 1993;76(4):919.
15. Zhu M, *et al*. Synthesis and annealing effects on the optical spectroscopy properties of red-emitting Gd(P0.5V0.5)O4: x at.% Eu3+. Journal of Materials Science: Materials in Electronics. 2018 Dec 1;29(24):20607-14. doi: 10.1007/s10854-018-0198-3.
16. Zhang S, Kono T, Ito A, Yasaka T, Uchiike H. Degradation mechanisms of the blue-emitting phosphor BaMgAl10O17: Eu2+ under baking and VUV-irradiating treatments. Journal of Luminescence. 2004 Jan 1;106(1):39-46. doi: 10.1016/S0022-2313(03)00132-7.
17. Zhang H, Fu X, Niu S, Sun G, Xin Q. Photoluminescence of YVO4: Tm phosphor prepared by a polymerizable complex method. Solid State Communications. 2004 Nov 1;132(8):527-31. doi: 10.1016/j.ssc.2004.09.008.
18. Chen G, Ohulchanskyy TY, Kumar R, Agren H, Prasad PN. Ultrasmall monodisperse NaYF4: *Yb3+/Tm3+ nanocrystals with enhanced near-infrared to near-infrared upconversion photoluminescence. ACS Nano. 2010 Jun 22;4(6):3163-8. doi: 10.1021/nn100457j.
19. Liao J, Qiu B, Wen H, Chen J, You W, Liu L. Synthesis process and luminescence properties of Tm3+ in AWO4 (A = Ca, Sr, Ba) blue phosphors. Journal of Alloys and Compounds. 2009 Nov 13;487(1):758-62. doi: 10.1016/j.jallcom.2009.08.068.
20. Wang J, Zhang ZJ. Luminescence properties and energy transfer studies of color-tunable Tb3+-doped RE1/3Zr2(PO4)3 (RE = Y, La, Gd and Lu). Journal of Alloys and Compounds. 2016 Nov 15;685:841-7. doi: 10.1016/j.jallcom.2016.06.224.
21. Okram R, Yaiphaba N, Ningthoujam RS, Singh NR. Is higher ratio of monoclinic to tetragonal in LaVO4 a better luminescence host? Redispersion and polymer film formation. Inorganic Chemistry. 2014 Jul 21;53(14):7204-13. doi: 10.1021/ic500828s.
22. Xia Z, Chen D, Yang M, Ying T. Synthesis and luminescence properties of YVO4:Eu3+,Bi3+ phosphor with enhanced photoluminescence by Bi3+ doping. Journal of Physics and Chemistry of Solids. 2010 Mar 1;71(3):175-80. doi: https://doi.org/10.1016/j.jpcs.2009.10.016.
23. Kang F, *et al*. Band-gap modulation in single Bi3+-doped yttrium–scandium–niobium vanadates for color tuning over the whole visible spectrum. Chemistry of Materials. 2016 Apr 26;28(8):2692-703. doi: 10.1021/acs.chemmater.6b00277.
24. Ullah S, *et al*. Synthesis and luminescence properties of La(P1-yVy)O4: X at.% Tm3+ as a blue emitting with high color purity phosphors. Journal of Physics and Chemistry of Solids. 2020 Sep 1;144:109485. doi: https://doi.org/10.1016/j.jpcs.2020.109485.
25. Song J, Gao Z, Chen G. Novel Tm3+/Dy3+ co-doped CaMoO4 transparent glass-ceramic phosphor for white LED applications. Journal of Alloys and Compounds. 2024 Dec 15;1008:176552. doi: https://doi.org/10.1016/j.jallcom.2024.176552.

26. Che D, *et al*. A facile aqueous strategy for the synthesis of high-brightness LaPO4:Eu nanocrystals via controlling the nucleation and growth process. Journal of Luminescence. 2014 Sep 1;153:369-74. doi: https://doi.org/10.1016/j.jlumin.2014.03.028.
27. Ullah S, *et al*. Co-precipitation synthesis and photoluminescence properties of (GdxLa1-x)PO4:5 at.%Eu3+ orange-red emitting phosphors. Journal of Materials Science: Materials in Electronics. 2019 Aug 1;30(15):14703-13. doi: 10.1007/s10854-019-01842-8.
28. Huittinen N, Arinicheva Y, Schmidt M, Neumeier S, Stumpf T. Using Eu3+ as an atomic probe to investigate the local environment in LaPO4–GdPO4 monazite end-members. Journal of Colloid and Interface Science. 2016 Dec 1;483:139-45. doi: https://doi.org/10.1016/j.jcis.2016.08.027.
29. Huittinen N, Arinicheva Y, Kowalski PM, Vinograd VL, Neumeier S, Bosbach D. Probing structural homogeneity of La1-xGdxPO4 monazite-type solid solutions by combined spectroscopic and computational studies. Journal of Nuclear Materials. 2017 Apr 1;486:148-57. doi: https://doi.org/10.1016/j.jnucmat.2017.01.024.
30. Li H, Jia G, Meng Z, Guo Q, Bai Y, Zhang C. Facile synthesis, multimode and tunable luminescence, and multifunctional applications of rare earth ions activated lead-free double perovskite crystals. Journal of Rare Earths. 2024 Sep 27. doi: https://doi.org/10.1016/j.jre.2024.09.028.
31. Zhang H, Zhang H. Special Issue: Rare earth luminescent materials. Light: Science & Applications. 2022 Sep 2;11(1):260. doi: 10.1038/s41377-022-00956-9.
32. George A, *et al*. Electronic structure and luminescence characteristics of rare earth free self-activated Ca2Sb2O7 blue emitting phosphor. Current Applied Physics. 2022 Jul 1;39:272-82. doi: https://doi.org/10.1016/j.cap.2022.05.007.
33. Kumar V, Tiwari SP, Ntwaeaborwa OM, Swart HC. 10 - Luminescence properties of rare-earth doped oxide materials. In: Dhoble SJ, Pawade VB, Swart HC, Chopra V, editors. Spectroscopy of Lanthanide Doped Oxide Materials. Woodhead Publishing; 2020. p. 345-64.
34. Jose TA, Gopinath A, Oommen SA, Joseph C, Biju PR. Novel Eu3+ doped Li2ZnTi3O8 phosphor: Synthesis, structural and optical characterization for white light emitting diodes. Journal of Molecular Structure. 2024 Jun 15;1306:137713. doi: https://doi.org/10.1016/j.molstruc.2024.137713.
35. Wang W, Li Z, Wu K, Wang Y, Liu Q. Synthesis, structure, and luminescence properties of Y2(MoO4)3:Eu3+ red phosphors for white light-emitting diodes. Journal of Alloys and Compounds. 2025 Mar 10;1019:179327. doi: https://doi.org/10.1016/j.jallcom.2025.179327.
36. Ullah S, *et al*. Optimizing photoluminescence properties of (Gd0.5La0.5)PO4:Eu0.05 phosphors through Al3+ ion doping. Optical Materials. 2025 Feb 1;159:116579. doi: https://doi.org/10.1016/j.optmat.2024.116579.
37. Weinstock N, Schulze HG, Müller A. Assignment of ν2 (E) and ν4 (F2) of tetrahedral species by the calculation of the relative Raman intensities: The vibrational spectra of VO43−, CrO42−, MoO42−, WO42−, MnO4−, TcO4−, ReO4−, RuO4, and OsO4. Journal of Chemical Physics. 1973;59:5063-67.
38. Seeta Rama Raju G, *et al*. Blue and green emissions with high color purity from nanocrystalline Ca2Gd8Si6O26:Ln (Ln=Tm or Er) phosphors. Journal of Alloys and Compounds. 2011 Jul 7;509(27):7537-42. doi: https://doi.org/10.1016/j.jallcom.2011.04.122.
39. Li Y-C, Chang Y-H, Lin Y-F, Lin Y-J, Chang Y-S. High color purity phosphors of LaAlGe2O7 doped with Tm3+ and Er3+. Applied Physics Letters. 2006;89:081110.
40. Rao GM, Seeta Rama Raju G, Hussain SK, Pavitra E, Rao PSVS, Yu JS. Tunable emissions via the white region from Sr2Gd8(SiO4)6O2:RE3+ (RE3+: Dy3+, Tm3+, Eu3+) phosphors. New Journal of Chemistry. 2016;40(7):6214-27. doi: 10.1039/C6NJ00017G.
41. Zhang S, Zhang P, Huang Y, Seo HJ. Self-activated emission and spectral temperature-dependence of Gd8V2O17 phosphor. Journal of Luminescence. 2019 Mar 1;207:460-464. doi: 10.1016/j.jlumin.2018.11.054.
42. Venikouas GE, Powell RC. Laser time-resolved spectroscopy: Investigations of energy transfer in Eu3+ and Er3+ doped YVO4. Journal of Luminescence. 1978 Jan 1;16(1):29-45. doi: 10.1016/0022-2313(78)90004-2.
43. Vistovskyy V, *et al*. Recombination luminescence in LaPO4-Eu and LaPO4-Pr nanoparticles. In: 2012 IEEE International Conference on Oxide Materials for Electronic Engineering (OMEE); 2012 Sept 3-7; pp. 219-220. doi: 10.1109/OMEE.2012.6464752.
44. Wu X, *et al*. Vacuum ultraviolet optical properties of (La,Gd)PO4:RE3+ (RE=Eu, Tb). Materials Research Bulletin. 2002 Aug 8;37(9):1531-1538. doi: 10.1016/S0025-5408(02)00860-7.
45. Wang L, Zhang W, Li Q, Wu G, Zhang Y, Jin D. The effect of M (Li+, K+, Mg2+, Al3+) ions on the quantum efficiency of YBO3:Eu3+ phosphors. Optik. 2020 Apr 1;207:163787. doi: 10.1016/j.ijleo.2019.163787.
46. Cho YS, Huh YD. Preparation and photoluminescence properties of red-emitting SrMoO4:Eu nanophosphor microcapsules. Electronic Materials Letters. 2015 Nov 1;11(6):1102-1108. doi: 10.1007/s13391-015-5184-9.
47. Lee JH, Heo MH, Kim SJ, Nahm S, Park K. Photoluminescence properties of (Y1−x−yMxEuy)BO3 (M=Al, Zn, and La) phosphors prepared by ultrasonic spray pyrolysis under VUV excitation. Journal of Alloys and Compounds. 2009 Apr 3;473(1):272-274. doi: 10.1016/j.jallcom.2008.05.091.
48. Cervantes-Juárez E, *et al*. Spectroscopy evaluation of crystalline and amorphous Cd2V2O7 as blue phosphors. Journal of Luminescence. 2018 Mar 1;195:234-239. doi: 10.1016/j.jlumin.2017.11.030.
49. Zeng S, *et al*. Composition design of fullerene-based hybrid electron transport layer for efficient and stable wide-bandgap perovskite solar cells. Journal of Energy Chemistry. 2025 Mar 1;102:172-178. doi: 10.1016/j.jechem.2024.10.046.
50. Wang L, Tan W. Multicolor FRET silica nanoparticles by single wavelength excitation. Nano Letters. 2006 Jan;6(1):84-88. doi: 10.1021/nl052105b.
51. Shen D, *et al*. Morphology/phase controllable synthesis of monodisperse ScVO4 microcrystals and tunable multicolor luminescence properties in Sc(La)VO4(PO4):Bi3+,Ln3+ phosphors. CrystEngComm. 2018;20(35):5180-5190. doi: 10.1039/C8CE00951A.
52. Park K, Nam SW. Red-emitting (Y0.5Gd0.5)0.94−xAlxEu0.06VO4 (0≤x≤0.04)

phosphors for plasma display panel applications. Optical Materials. 2010 Mar 1;32(5):612-615. doi: 10.1016/j.optmat.2009.12.008.
53. Madhu M, Rao AV, Murali N, Parajuli D, Mammo TW. Effect of Al3+ substitution on the synthesis, magnetic, and electrical properties of Ni0.3Zn0.5Co0.2Fe2−xAlxO4 spinel ferrites. Journal of Materials Science: Materials in Electronics. 2023 Nov 15;34(32):2158. doi: 10.1007/s10854-023-11551-y.
54. Liao Z, Zhang Q, Qiu L, Wei X, Chen Y, Yin M. CaLuGaO4:Bi3+,Al3+ blue phosphor with excellent thermal stability for multiple LED applications. Journal of Materials Chemistry C. 2025;13(10):5221-5231. doi: 10.1039/D4TC05004E.
55. Marques dA, Künzel R, Umisedo NK, Latini RM, Yoshimura EM, Okuno E. Tm3+ doped barium molybdate: A potential long-lasting blue phosphor. Journal of Alloys and Compounds. 2018 Feb 25;735:707-717. doi: 10.1016/j.jallcom.2017.10.225.
56. Liao J, Qiu B, Wen H, You W, Xiao Y. Synthesis and optimum luminescence of monodispersed spheres for BaWO4-based green phosphors with doping of Tb3+. Journal of Luminescence. 2010 May 1;130(5):762-766. doi: 10.1016/j.jlumin.2009.11.028.
57. Zheng J, *et al*. Structure, electronic properties, luminescence and chromaticity investigations of rare earth doped KMgBO3 phosphors. Materials Chemistry and Physics. 2015 Sep 1;165:168-176. doi: 10.1016/j.matchemphys.2015.09.012.
58. Liu WR, Huang CH, Wu CP, Chiu YC, Yeh YT, Chen TM. High efficiency and high color purity blue-emitting NaSrBO3:Ce3+ phosphor for near-UV light-emitting diodes. Journal of Materials Chemistry. 2011;21(19):6869-6874. doi: 10.1039/C1JM10765H.
59. Feng Y, *et al*. Effect of PO43−/VO43− proportion on structure and photoluminescence properties of Gd(PyV1−y)O4: X at.% Tm3+ phosphors. Journal of Luminescence. 2020 Jan 1;217:116796. doi: 10.1016/j.jlumin.2019.116796